

How cosmic-ray electron propagation affects radio – far-infrared correlations in M 31 and M 33

E. M. Berkhuijsen¹ \star , R. Beck¹ and F. S. Tabatabaei²

¹MPI für Radioastronomie, Auf dem Hügel 69, 53121 Bonn, Germany

²MPI für Astronomie, Königstuhl 17, 69117 Heidelberg, Germany

Accepted 2013 July 26. Received 2013 July 13; in original form 2013 January 18

ABSTRACT

We investigate the effect of propagation of cosmic-ray electrons (CRE) on the nonthermal (synchrotron) – far-infrared correlations in M 31 and M 33. The thermal (TH) and non-thermal (NTH) emission components of the radio continuum emission at 1.4 GHz and one higher frequency are compared with dust emission from M 31 and M 33 using Spitzer data. In both galaxies the TH emission is linearly correlated with the emission from warm dust ($24\ \mu\text{m}$, $70\ \mu\text{m}$), but the power laws of the NTH – FIR correlations have exponents $b < 1$ that increase with increasing frequency. Furthermore, the values of b for M 33 are significantly smaller ($b \approx 0.4$) than those for M 31 ($b \approx 0.6$). We interpret the differences in b as differences in the diffusion length of the CRE. We estimate the diffusion length in two ways: (1) by smoothing the NTH emission at the higher frequency until the correlation with NTH emission at 1.4 GHz has $b = 1$, and (2) by smoothing the TH emission until the correlation with the NTH emission at the same frequency has $b = 1$, assuming that the TH emission represents the source distribution of the CRE. Our smoothing experiments show that M 31 only has a thin NTH disk with a scale height of $h = 0.3 - 0.4$ kpc at 1.4 GHz, whereas M 33 has a similar thin disk as well as a thick disk with scale height $h_{\text{thick}} \approx 2$ kpc. In the thin disks, the (deprojected) diffusion length at 1.4 GHz is ≈ 1.5 kpc, yielding a diffusion coefficient of $\approx 2 \cdot 10^{28}$ cm²/s. The structure, strength and regularity of the magnetic field in a galaxy as well as the existence of a thick disk determine the diffusion of the CRE, and hence, the power-law exponent of the NTH – FIR correlations.

Key words: galaxies: individual: M 31 – galaxies: individual: M 33 – galaxies: spiral – galaxies: cosmic rays – galaxies: magnetic fields – infrared: galaxies – radio continuum: galaxies

1 INTRODUCTION

The radio continuum and far-infrared (FIR) luminosities of star-forming galaxies are tightly correlated over five orders of magnitude (e.g. de Jong et al. (1985); Helou, Soifer & Rowan-Robinson (1985); Condon (1992); Yun, Reddy & Condon (2001)). The correlation is nearly linear and probably arises because both emissions depend on the recent star-formation rate in a galaxy. Massive stars heat the dust and ionize the gas causing thermal dust emission and thermal (free-free) radio continuum emission, respectively. These stars are progenitors of supernova remnants, which are the sources of cosmic ray electrons (CRE) that radiate nonthermal (synchrotron) emission when spiraling around magnetic field lines. Attempts to explain the correlation were made by Völk (1989); Helou & Bica (1993); Niklas & Beck (1997) and Hoernes, Berkhuijsen & Xu (1998). Recently, Bell (2003) and Lacki & Thompson (2010) showed that several factors conspire in making the global correlation linear over five decades.

The radio – FIR correlation¹ also holds within star-forming galaxies down to scales of below hundred parsec (e.g. Beck & Golla (1988); Bica, Helou & Condon (1989); Fitt et al. (1992); Xu et al. (1992); Lu et al. (1996); Hoernes, Berkhuijsen & Xu (1998); Hippelein et al. (2003); Hughes et al. (2006); Paladino et al. (2006); Dumas et al. (2011); Leverenz & Filipović (2012); Tabatabaei et al. (2013b)). However, many authors (starting with Xu et al. (1992)) found that the radio – FIR correlation within galaxies only becomes linear on star-forming regions but is non-linear, usually with power-law exponent < 1 , in other parts of a galaxy. Separation of thermal/nonthermal radio emission and of warm/cool dust emission revealed that the thermal radio – warm dust correlation is linear, whereas the nonthermal radio-cool dust correlation has an exponent $\neq 1$ (Xu et al. 1992; Hoernes, Berkhuijsen & Xu 1998; Hippelein et al. 2003; Basu, Roy & Mitra 2012). This explains why the radio – FIR correlation of the total emission steepens on star-forming

\star E-mail: eberkhuijsen@mpifr-bonn.mpg.de

¹ Throughout this paper, the radio and FIR intensities are on the Y- and X-axis, respectively.

regions where the thermal fraction of the radio emission is high (Hughes et al. 2006; Paladino et al. 2006; Dumas et al. 2011). The smaller exponent of the nonthermal – FIR correlation is probably due to diffusion of the CRE away from their places of origin. By smoothing images of warm dust emission until they resembled those of radio emission at 1.4 GHz propagation lengths of up to several kpc were found (Bicay & Helou (1990); Marsh & Helou (1998); Murphy et al. (2006a,b, 2008, 2012)).

On each of our nearest spiral galaxies, M 31 and M 33, one radio – FIR study is available. The radio – FIR correlation within M 31 was extensively studied by Hoernes, Berkhuijsen & Xu (1998), who were the first to separate thermal/nonthermal emission at 1.4 GHz and warm/cool dust emission using HIRES data. By means of classical, pixel-to-pixel correlations and rigorous statistics they found significant relationships between thermal radio and warm dust emission and between nonthermal radio and cool dust emission, with power-law exponents of 1.2 ± 0.1 and 0.8 ± 0.1 , respectively.

Hippelein et al. (2003) studied the dust distribution in M 33 observed by ISOPHOT. They also plotted the total 4.8 GHz luminosity of star-forming regions against that of the total FIR and obtained a power law with exponent 0.9. The exponent is < 1 because 30–40% of the 4.8 GHz emission from these regions is nonthermal (Tabatabaei et al. 2007b). Below we compare radio – FIR correlations in M 31 and M 33 using new thermal and nonthermal radio maps and recent FIR data.

Tabatabaei et al. (2007b) obtained the distribution of the thermal emission at 21.0 cm (1425 MHz) and 3.6 cm (8350 MHz) from M 33 from the extinction-corrected $H\alpha$ map of Hoopes & Walterbos (2000). The extinction correction was based on the optical depth map derived from Spitzer MIPS data at $70 \mu\text{m}$ and $160 \mu\text{m}$ presented by Tabatabaei et al. (2007a). By subtracting the corrected thermal emission from the total radio emission observed by Tabatabaei et al. (2007a), they obtained the distributions of the nonthermal emission across M 33 at 21 cm and 3.6 cm. This new method of separating thermal/nonthermal radio emission from a galaxy is preferable above the standard method, which requires the unrealistic assumption of a constant nonthermal spectral index between the radio emissions at two wavelengths.

Recently, Tabatabaei & Berkhuijsen (2010) derived an optical depth map of M 31 from the $70 \mu\text{m}$ and $160 \mu\text{m}$ Spitzer MIPS maps of Gordon et al. (2006) and used this to correct the $H\alpha$ map of Devereux et al. (1994) for extinction. Taking the gradient in electron temperature into account, we converted this map to distributions of thermal emission at 20.5 cm (1465 MHz) and 6.3 cm (4850 MHz). Subtraction of the thermal emission from the total emission at the corresponding wavelength (Beck et al. 1998; Berkhuijsen et al. 2003) then yielded the distributions of the non-thermal emission at 20.5 cm and 6.3 cm. The details of this procedure are described in Tabatabaei et al. (2013a) where also the thermal and non-thermal maps at 1.4 GHz of both galaxies are shown.

In this paper we correlate the new thermal and nonthermal distributions of M 31 and M 33 with the distributions of the dust emission. We discuss the differences in the correlation results for the two galaxies focussing on the diffusion of CRE. The correlations and statistics are presented in Sect. 2. We derive diffusion lengths of CRE in the plane of the sky in Sect. 3 and discuss these results in Sect. 4. In Sect. 5 we describe the propagation of CRE within and perpendicular to the disk of each galaxy, and we discuss the role of star formation and magnetic fields in Sect. 6. We compare with earlier work on CRE propagation in Sect. 7 and summarize our conclusions in Sect. 8.

Throughout the paper, we assume a distance $D = 780$ kpc (Stanek & Garnavich 1998) and inclination $i = 75^\circ$ for M 31, and $D = 840$ kpc (Freedman, Wilson & Madore 1991) and $i = 56^\circ$ for M 33.

2 CLASSICAL CORRELATIONS BETWEEN RADIO AND DUST EMISSIONS

For a fair comparison of the radio – FIR correlations in M 31 and M 33, we selected regions that contain a range of star-formation rates and are fully covered by all data sets. This is the case for the bright “ring” of emission in M 31 in the radial range $R = 6.8$ kpc–12.5 kpc ($30' - 55'$) and in M 33 at radii $R < 5$ kpc ($< 20.5'$). For M 31 we made correlations at the angular resolution of $45''$ (corresponding to 170 pc \times 660 pc along the major and minor axis in the plane of the galaxy) of the 20.5 cm data and at the resolution of $3'$ (680 pc \times 2630 pc) of the 6.3 cm data. The dust maps were smoothed to the resolutions of the radio maps by using the custom kernels presented by Gordon et al. (2007). All data for M 33 were smoothed to the resolution of $90''$ (370 pc \times 655 pc) of the 3.6 cm data. We note that the angular resolution does not affect the correlation results, provided it is the same for the data sets correlated.

We made pixel-to-pixel correlations between the distributions of the thermal emission (TH) and those of the dust emission at $24 \mu\text{m}$, $70 \mu\text{m}$ and $160 \mu\text{m}$ as well as between the distributions of the non-thermal emission (NTH) and those of the dust emission. Only pixels with intensities above $2 \times$ rms noise were used. We obtained sets of independent data points, i.e. a beam area overlap of $< 5\%$, by choosing pixels spaced by more than $1.67 \times$ the beamwidth. Since the correlated variables are not directly depending on each other, we fitted a power law by determining the OLS bisector in the log-log plane in each case (Isobe et al. 1990).

We also calculated the correlation coefficient, r_c , to show how well two components are correlated, and the student-t test (Wall 1979) to indicate the statistical significance of the fit. For a number of independent points of $N > 60$, the fit is significant at the 3σ level if $t > 3.1$. Errors in intercept a and slope b of the bisector are standard deviations (1σ). The bisector fits of the correlations for M 31 and M 33 are given in Tables 1 and 2, respectively.

In Fig. 1 we present examples of scatter plots between radio and dust emission for both galaxies. The correlations between thermal radio emission at 21 cm and warm dust emission at $24 \mu\text{m}$ are close to linear (Fig. 1a). This is not surprising as both emissions are powered by massive stars. The power-law exponent of $b = 1.08 \pm 0.02$ for M 31 (Table 1) is consistent with the value of 1.2 ± 0.1 found by Hoernes, Berkhuijsen & Xu (1998). Xu et al. (1992) derived a linear relationship between thermal emission at 6.3 cm and warm dust emission for the Large Magellanic Cloud.

Figure 1a shows that the thermal emission from M 31 is weaker than that from M 33, which is due to its smaller star formation rate per kpc^2 (Tabatabaei & Berkhuijsen 2010). However, the same amount of thermal emission corresponds to 70% more $24 \mu\text{m}$ emission from M 31 than from M 33. This indicates that a significant part of the $24 \mu\text{m}$ emission from the “bright ring” in M 31 originates from sources other than warm dust heated by massive stars. Tabatabaei & Berkhuijsen (2010) arrived at the same conclusion based on an excess in the $24 \mu\text{m}/70 \mu\text{m}$ emission ratio.

For both galaxies the correlation between thermal emission and emission from cool dust seen at $160 \mu\text{m}$ is non-linear with exponent $b = 1.4$ (Tables 1 and 2). Since the cool dust is mainly heated by the diffuse interstellar radiation field (ISRF) (Xu et al.

Table 1. M 31: Classical correlations between FIR and radio emission for $6.8 < R < 12.5$ kpc. OLS bisector fits with N the number of independent data points, r_c the correlation coefficient and t student-t test.

X [MJy/sr]	Y [μ Jy/kpc ²]	log(Y)=a+b*log(X)		N	Corr. Coeff. r_c	t
		a	b			
I(24)	TH(20.5)	4.18±0.01	1.08±0.02	1036	0.77±0.02	39
I(70)	TH(20.5)	3.20±0.01	0.99±0.02	1023	0.78±0.02	40
I(160)	TH(20.5)	1.91±0.04	1.42±0.03	1047	0.77±0.02	38
I(24)	NTH(20.5)	4.62±0.01	0.61±0.02	1093	0.67±0.02	29
I(70)	NTH(20.5)	4.07±0.01	0.56±0.01	1079	0.67±0.02	30
I(160)	NTH(20.5)	3.34±0.03	0.78±0.02	1105	0.67±0.02	30
I(24)	NTH(6.3)	4.46±0.03	0.97±0.09	65	0.54±0.11	5
I(70)	NTH(6.3)	3.56±0.06	0.87±0.08	65	0.56±0.11	5
I(160)	NTH(6.3)	2.48±0.16	1.21±0.11	65	0.58±0.10	6
TH(20.5)	NTH(20.5)	2.11±0.04	0.61±0.02	1044	0.51±0.03	19
TH(6.3)	NTH(6.3)	0.93±0.27	0.84±0.08	64	0.41±0.12	4

Note: Correlations between TH(6.3) and dust emission agree within errors with those between TH(20.5) and dust emission.

Table 2. M 33: Classical correlations between FIR and radio emission for $R < 5$ kpc. OLS bisector fits with N the number of independent data points, r_c the correlation coefficient and t student-t test.

X [MJy/sr]	Y [μ Jy/kpc ²]	log(Y)=a+b*log(X)		N	Corr. Coeff. r_c	t
		a	b			
I(24)	TH(21)	4.41±0.02	1.06±0.04	158	0.89±0.04	25
I(70)	TH(21)	3.03±0.03	1.20±0.04	160	0.91±0.03	27
I(160)	TH(21)	2.21±0.07	1.40±0.05	160	0.87±0.04	23
I(24)	NTH(21)	4.62±0.01	0.35±0.02	159	0.75±0.05	14
I(70)	NTH(21)	4.17±0.01	0.39±0.02	161	0.80±0.05	17
I(160)	NTH(21)	3.90±0.03	0.46±0.02	161	0.80±0.05	17
I(24)	NTH(3.6)	4.11±0.02	0.59±0.04	134	0.56±0.07	8
I(70)	NTH(3.6)	3.34±0.04	0.67±0.05	135	0.57±0.07	8
I(160)	NTH(3.6)	2.87±0.08	0.79±0.06	135	0.51±0.08	7
TH(21)	NTH(21)	2.84±0.05	0.34±0.02	160	0.69±0.06	12
TH(3.6)	NTH(3.6)	1.33±0.15	0.61±0.05	134	0.53±0.07	7

Note: Correlations between TH(3.6) and dust emission agree within errors with those between TH(21) and dust emission.

1992), its emission is much smoother than that of the ionized gas, leading to an exponent $b > 1$.

Figure 1b shows that for both galaxies the correlation between nonthermal emission at 21 cm and 160 μ m emission has a power-law exponent $b < 1$, but the exponents for the two galaxies are strikingly different. As the TH – 160 μ m correlations have the same value of b , the difference is in the character of the nonthermal emission that is much smoother in M 33 ($b = 0.46 \pm 0.02$) than in M 31 ($b = 0.78 \pm 0.02$) caused by the relatively high intensities towards lower brightness. This could mean that the propagation length of the CRE in M 33 is larger than in M 31 or that M 33 has a halo.

The smaller values of exponent b for M 33 than for M 31 are confirmed by the correlations between nonthermal emission at 21 cm and the emissions at 24 μ m and 70 μ m (Tables 1 and 2). In Tables 1 and 2 we have also listed the power-law fits of the correlations between nonthermal emission at 6.3 cm (M 31) or 3.6 cm (M 33) and dust emission. These have exponents much closer to 1, but the difference between M 31 and M 33 remains. Exponents closer to 1 imply less diffusion of CRE, which is expected at smaller wavelengths. Below we will employ the observed differ-

ences in the correlations to estimate the diffusion length of the CRE in the two galaxies.

3 DIFFUSION OF CR ELECTRONS

CR particles may propagate through the ISM by streaming with the Alfvén velocity along the ordered magnetic field lines or they may be scattered by the irregularities of the turbulent magnetic field, leading to random-walk diffusion along the ordered field. As in the Milky Way disk the latter process dominates (Strong, Moskalenko & Ptuskin 2007; Dogiel & Breitschwerdt 2012), we expect that in the disks of M 31 and M 33 the CRE also mainly propagate by diffusion.

In order to estimate the diffusion length of CRE, we need to know the total magnetic field strength, B_{tot} , in the galaxy disk, which determines the energy and the lifetime of the CRE (see Eqs. 2 and 3 below). We derive B_{tot} in Sect. 3.1 and the diffusion lengths of CRE in the plane of the sky in Sect. 3.2.

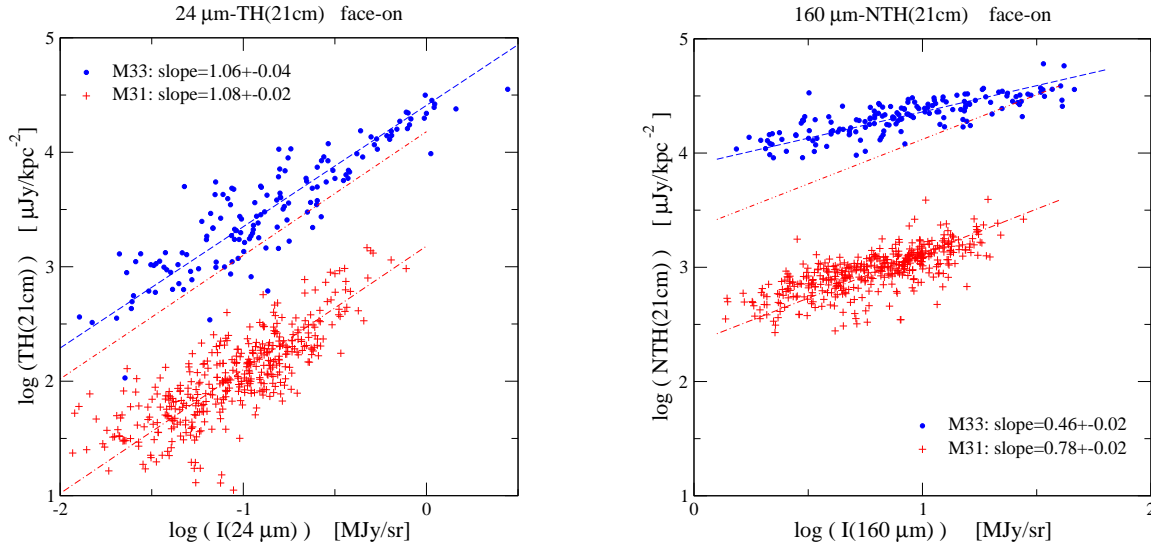


Figure 1. Scatter plots between the surface brightnesses of FIR emission and 21 cm radio continuum emission from M31 and M33. Dashed lines show the power-law fits given in Tables 1 and 2. The scatter plots for M31 are shifted down by a factor of 10 for clarity. The correct locations of the fits are shown by the red dashed lines just below the M33 plots. (a) Thermal emission at 21 cm versus $24\ \mu\text{m}$ emission. (b) Nonthermal emission at 21 cm versus $160\ \mu\text{m}$ emission. A colour version of this figure is shown in the electronic version of the paper.

3.1 Synchrotron scale heights and magnetic field strengths

We calculated the mean value of B_{tot} in the radial intervals used for the radio – FIR correlations (i.e. $R = 6.8 - 12.5$ kpc in M31, $R = 0 - 5$ kpc in M33) from the mean surface brightness of the nonthermal (synchrotron) emission using the code BFIELD of M. Krause² based on Eq. 3 of Beck & Krause (2005). This equation assumes energy equipartition between total cosmic rays and total magnetic fields. The code asks for the nonthermal spectral index α_n , the nonthermal degree of polarization, the line of sight through the medium L and the ratio of the number densities of protons and electrons K , here taken equal to 100. The value of α_n follows from the mean nonthermal intensities at the two frequencies used ($I \propto \nu^{-\alpha_n}$) giving $\alpha_n = 0.92 \pm 0.06$ for M31 and $\alpha_n = 0.86 \pm 0.08$ for M33 (see Table 6). The degree of polarization, i.e. polarized/nonthermal intensity, was calculated for the areas considered. The lines of sight were obtained from the exponential scale heights of the nonthermal emission estimated in the following way.

On the 21 cm nonthermal map of M31 at $45''$ resolution we measured the half-power width of several spiral arms in each quadrant of the bright emission ring along cuts parallel to the minor axis taken at $X = 25:5$, $23:0$ and $19:5$ on the northern major axis and $X = 14:5$, $17:0$ and $19:5$ on the southern major axis. Because of the high inclination of M31, the cuts are nearly perpendicular to the arms at these positions and the width of the arms on the sky plane is determined by their vertical extent. We converted the half-power widths, corrected for inclination and angular resolution, to exponential scale heights and calculated the radius R in the galaxy plane for each measured position. This yielded mean scale heights of $h = 300 \pm 25$ pc at $R = 8 - 10$ kpc and $h = 335 \pm 15$ pc at $R = 10 - 12$ kpc.

The mean exponential scale height in the radial interval $R = 6.8 - 12.5$ kpc, used for the radio – FIR correlations, was

estimated from the scale height of the total gas (HI + 2H_2). Berkhuijsen, Bajaja & Beck (1993) noted that the scale height of the total (mainly nonthermal) 21 cm emission is close to that of the total gas in arms in the SW quadrant of the “ring”. We checked this on the total gas map of Nieten et al. (2006), smoothed to $45''$ resolution, by measuring the half-power widths of the gas arms at the same positions as above. As we found a mean ratio of the nonthermal/gas scale heights of 0.88 ± 0.05 , the nonthermal scale height at 21 cm is indeed nearly equal to the total gas scale height. For the area $R = 6.8 - 12.5$ kpc, the mean scale height of the total gas is $h_{\text{gas}} \approx 330$ pc (calculated from the ratio mean column density / mean volume density (Tabatabaei & Berkhuijsen 2010), which is consistent with the nonthermal scale heights derived above. Therefore, we adopted $h_{\text{syn}} = 330 \pm 40$ pc for M31 giving an effective line of sight through the medium of $L = 2h_{\text{syn}} / \cos(i) = 2550 \pm 310$ pc.

For M33 we cannot measure the exponential scale height of the 21 cm nonthermal emission because at the inclination of 56° the arm widths in and perpendicular to the disk are superimposed on the sky plane. Therefore, we assumed the nonthermal scale height to be equal to the scale height of the total gas, as is the case in M31. Little information on the gas scale height in M33 exists in the literature. We calculated the mean HI scale height for $R < 20:5$ from the half thickness as function of radius given in Table II of Warner, Wright & Baldwin (1973), correcting for an erroneous factor $\sqrt{2}$ and taking the increase in the area of rings with increasing radius into account. For the distance $D = 840$ pc this gave $h_{\text{HI}} = 360$ pc. Heyer et al. (2004) found a relationship for the column density ratio $N(\text{HI})/N(\text{H}_2)$ with radius. Integration out to $R = 20:5$ yielded a mean value of 3.4 giving $N(\text{H}_2)/N(\text{HI}) = 0.29$. Assuming $h_{\text{H}_2} = h_{\text{HI}}/2$, we obtained a scale height of the total gas of $h_{\text{gas}} = 320$ pc. We adopted $h_{\text{syn}} = 320 \pm 80$ pc and $L = 1140 \pm 280$ pc for M33. Note that the uncertainty in L has little influence on the derived value of the magnetic field strength because it enters the calculation to the power $1/(3 + \alpha_n)$.

Our estimates of h_{syn} agree with scale heights obtained for other galaxies. Like in the Milky Way, observations of edge-

² www.mpifr-bonn.mpg.de/staff/mkrause

on galaxies usually reveal a thin synchrotron disk with a scale height of about 0.3 kpc and a thick synchrotron disk with a scale height of 1 – 2 kpc (Beuermann, Kanbach & Berkhuijsen 1985; Dumke & Krause 1998; Krause 2011). Thus our estimates of $h_{\text{syn}} \approx 330$ pc refer to the thin disks in M 31 and M 33.

The derived scale heights and total magnetic field strengths are summarized in Table 3 that also gives the scale heights of the CRE, $h_{\text{CRE}} = h_{\text{syn}}(3 + \alpha_n)/2$, and their energy E calculated from Eq. 3 in Sect. 3.2. The values of h_{CRE} at the high frequencies were scaled from those at 1.4 GHz with $\nu^{-0.125}$ (see below Eq. 4 in Sect. 3.2).

3.2 Diffusion lengths of CRE

Since the sources of CRE probably are supernova remnants (SNRs) located in or near star-forming regions, we used the distribution of the *thermal* emission as the source distribution of the CRE (see Fig. 2). We thus avoid the influence of dust properties and other heating sources than massive stars (e.g. evolved stars, the diffuse ISRF) that may play a role when the distribution of IR emission is taken as the source distribution. The relationships between nonthermal and thermal emission (given at the end of Tables 1 and 2) show the same trends as those between nonthermal and dust emission, i.e. exponents b increase with frequency, and for M 33 the exponents are smaller than for M 31. We interpret these trends as the result of differences in diffusion lengths of the CRE.

In the following we assume that CRE are injected into the ISM by SNRs shocks continuously (at least during a few times the CRE lifetime), leading to a stationary distribution of CRE in the galaxy. We further assume that the diffusion of the CRE leads to a Gaussian distribution of the CRE. The separation of the SNRs is larger than the diffusion length of the CRE in the disk and avoids overlap of diffusion lengths of CRE from neighbouring sources, which would otherwise influence the estimated mean diffusion length. Within a radius of 5 kpc from the centre, M 33 contains $\lesssim 40$ SNRs and SNR candidates of diameter $D \lesssim 30$ pc (Long et al. 2010), which are the main sources of CRE (Berezhko & Völk 2004). Their mean separation is 1.4 kpc, which is larger than the typical diffusion length of ≈ 1 kpc. As the star formation rate / area in the emission ring of M 31 is five times smaller than in M 33 (see Table 6), the mean separation of CRE sources in the ring is > 1.4 kpc. So it will be possible to estimate the CRE diffusion length in both galaxies.

The only difference between the nonthermal emissions from a galaxy at two frequencies is the diffusion length of CRE that is reached by random-walk diffusion, other variables like their source distribution and the magnetic field strength being the same. The diffusion length $l(\nu)$ at frequency ν is determined by the synchrotron life time t_{syn} and the diffusion coefficient $^3 D_E$. The mean synchrotron lifetime $\langle t \rangle$ of the bulk of CRE, a mixture of CRE of all ages, is smaller than t_{syn} ; it may be written as

$$\langle t \rangle = \int_0^{t_{\text{syn}}} N t dt / \int_0^{t_{\text{syn}}} N dt, \quad (1)$$

where N is the number of CRE as a function of time, $N = N_0 \exp[-t/t_{\text{syn}}]$. Evaluation of $\langle t \rangle$ yields $\langle t \rangle = t_{\text{syn}}(1 - 2/e) / (1 - 1/e) = 0.42 t_{\text{syn}}$. Therefore, we take $t_{\text{syn}}/2$ as the typical age of the bulk of the CRE in the calculations below. The diffusion length then is

$$(l_\nu/\text{pc})^2 \approx (D_{E,\nu}/\text{pc}^2 \text{ yr}^{-1}) (t_{\text{syn}}/2)/10^7 \text{ yr}. \quad (2)$$

$D_{E,\nu}$ depends on the energy E of the CRE as $D_{E,\nu} \propto E^p$, where $p \approx 0.5$ (Strong, Moskalenko & Ptuskin 2007). E is related to the radiating frequency:

$$(\nu/\text{GHz}) \approx 1.3 \cdot 10^{-2} (B_{\text{tot}}/\mu\text{G}) (E/\text{GeV})^2, \quad (3)$$

where B_{tot} is the total magnetic field strength derived from the surface brightness of the nonthermal emission. Mean values of B_{tot} and E for the regions used for the correlations are given in Table 3.

The lifetime of the radiating CRE is mainly determined by the synchrotron losses at our frequencies (e.g. Fig. 1 in Murphy (2009)):

$$(t_{\text{syn}}/10^7 \text{ yr}) \approx 1.4 \cdot 10^9 (\nu/\text{GHz})^{-0.5} (B_{\text{tot}}/\mu\text{G})^{-1.5}. \quad (4)$$

Thus, at high ν we see radiation from younger electrons than at low ν , and because of their shorter lifetime they cannot travel as far as those at low ν , in spite of their higher energy. Comparing Eqs. 1, 2, and 3, we see that for a fixed value of B_{tot} , $l_\nu^2 \propto \nu^{-0.25}$, if $D_{E,\nu} \propto E^{0.5}$. An estimate of l_ν^2 yields an estimate of $D_{E,\nu}$ from Eq. 2.

We measured the diffusion length in the plane of the sky in two ways: (1) by determining the difference in diffusion length between 1.4 GHz and the higher frequency, and (2) by estimating the diffusion length at each frequency separately using the distribution of the thermal emission as the source distribution of the CRE.

1. The most direct way to measure the average diffusion length of CRE is a comparison of the nonthermal distributions at the two frequencies. Since the CRE radiating at the higher frequency are still closer to their origin than at 1.4 GHz, smoothing of the *non-thermal* distribution at the higher frequency will make it more similar to that at 1.4 GHz. We smoothed the high-frequency distributions until the power-law exponent of the correlation with the nonthermal distribution at 1.4 GHz had $b = 1$, indicating that the two distributions are most similar. The smoothing beam required for this, corrected for the resolution of the observations, represents the difference in diffusion length between the two frequencies.

Because distances are measured from the centre of the telescope beam, we took half of the full width at half power of the corrected smoothing beam as the derived difference in the square of the diffusion lengths, Δl^2 . Then, using Eq. 1 and $\Delta l^2 = l_{1.4}^2 - l_\nu^2$, we have

$$\Delta l^2 \approx l_{1.4}^2 (1 - (\nu/1.4 \text{ GHz})^{-0.25}), \quad (5)$$

where $l_{1.4}$ is the diffusion length at 1.4 GHz. From the derived value of $l_{1.4}^2$ we obtain l_ν^2 by scaling with $\nu^{-0.25}$. The resulting diffusion lengths observed in the plane of the sky, l_{sky} , are given in Table 4. The errors are determined by the standard deviations in b of the correlations giving the best smoothing beam.

2. The exponents b of the nonthermal–thermal correlations are < 1 because the CRE diffused away from their places of origin represented by the distribution of the thermal emission (see Sect. 4 and Fig. 2). We obtained an estimate of the diffusion length at each frequency by smoothing the *thermal* emission until the exponent of the correlation with the nonthermal emission at that frequency became $b = 1$. By requiring $b = 1$, we implicitly assume that $B_{\text{tot}}^{1+\alpha_n}$ is about constant within the area considered ($I_{\text{NTH}} \propto N_{\text{CRE}} B_{\text{tot}}^{1+\alpha_n}$). On large scales this is approximately the case as radial variations in B_{tot} are $< 10\%$ in the areas used for the correlations (i.e. see Fig. 9 in Tabatabaei et al. (2008)). Small-scale variations in B_{tot} will only contribute to the spread in the data points. Again, we took half the corrected smoothing beam as the diffusion length in the sky plane to obtain the diffusion lengths given in Table 4.

³ $1 \text{ pc}^2 \text{ yr}^{-1} \approx 30.2 \cdot 10^{28} \text{ cm}^2 \text{ sec}^{-1}$

Table 3. Exponential scale heights and magnetic field strengths of the thin disks in M31 and M33

Galaxy	R [kpc]	Frequency [GHz]	h_{syn} [pc]	h_{CRE}^a [pc]	B_{tot} [μG]	E [GeV]	$t_{\text{syn}}/2$ [10^7 yr]
M31	6.8-12.5	1.465	330 ± 40	650 ± 80	6.6 ± 0.3	4.1	3.4 ± 0.2
		4.85	–	560 ± 70^b	6.6 ± 0.3	7.5	1.9 ± 0.1
M33	0 - 5	1.425	320 ± 80^c	620 ± 150	8.1 ± 0.5	3.7	2.5 ± 0.2
		8.35	–	500 ± 120^b	8.1 ± 0.5	8.9	1.1 ± 0.1

(a) $h_{\text{CRE}} = h_{\text{syn}} (3 + \alpha_n)/2$ (b) Scaled from $h_{\text{CRE}}(1.4 \text{ GHz})$ with $\nu^{-0.125}$ (see Eq. 4)

(c) Assumed to be equal to the gas scale height like in M31

Table 4. Observed diffusion lengths of CRE in M31 and M33 on the sky

Galaxy	Method	Frequency [GHz]	l_{sky} [pc]
M31	1	1.465	1140 ± 190^a
		4.85	980 ± 160^b
	2	1.465	715 ± 20
		4.85	510 ± 60
M33	1	1.425	900 ± 110^a
		8.35	720 ± 90^b
	2	1.425	1960 ± 170
		8.35	1450 ± 200

(a) Based on the observed difference in diffusion length between two frequencies (see Eq. 4):

M31: $(\Delta l^2)^{0.5} = 580 \pm 100$ pc; M33: $(\Delta l^2)^{0.5} = 540 \pm 65$ pc(b) Scaled from 1.4 GHz with $l_{\text{sky}} \propto \nu^{-0.125}$

In both cases we used circular Gaussian smoothing beams because they gave the best fits. Even for the highly inclined galaxy M31, fits with elliptical beams parallel to the major axis were worse than those with circular beams. This agrees with the results of Marsh & Helou (1998) who found circular smoothing beams optimal for 10 out of 16 galaxies. Hence, in these galaxies the deprojected diffusion lengths within the disk and perpendicular to the disk are about the same (see Sect. 5).

4 DIFFUSION LENGTHS IN THE PLANE OF THE SKY

The observed diffusion lengths in Table 4 are in the range 0.5–2 kpc in the plane of the sky (measured along the major axis). At each frequency, the two methods yield diffusion lengths that agree within a factor of 2. Method 2 yields smaller values than method 1 for M31, but larger values for M33. The estimates by the two methods may differ for several reasons.

a) Method 1 measures the difference in diffusion length between the two frequencies. Since the lifetime of the CRE at the higher frequency is about half of those at 1.4 GHz (see Table 3), they do not propagate as far as those at 1.4 GHz. This means that the diffusion length of the older CRE emitting at 1.4 GHz, which had time to propagate far from their places of origin, determines Δl^2 . Hence, Δl^2 is an upper limit to the mean diffusion length of the bulk of CRE. If older CRE not only propagate along the disk but also move out of the thin disk into a thick disk / halo, the “vertical” propagation length may add to the diffusion length observed in the thin

disk by an amount depending on the inclination. However, observations of edge-on galaxies show that CRE propagation out of the thin disk usually occurs in SF regions (i.e. Dahlem, Dettmar & Hummel (1994); Dumke et al. (1995); Heesen et al. (2009)) and most of these CRE will be young (Breitschwerdt, Dogiel & Völk 2002). Therefore we expect that method 1 estimates an upper limit to the diffusion length at 1.4 GHz that mainly refers to the thin disk.

b) Method 2, however, measures the mean diffusion length of the bulk of the CRE, i.e. of a mixture of CRE of all ages, at each frequency. The inclusion of young CRE will yield a diffusion length smaller than the upper limit from method 1, consistent with our results for M31. Furthermore, method 2 includes the full effect of CRE propagation out of the thin disk. If this is significant, the observed diffusion length could be larger than the estimate from method 1, as we find for M33. We discuss the evidence for a thick disk / halo in M33 in Sect. 5.2.

c) Method 2 is based on the assumption that the source distribution of the CRE is similar to that of the thermal emission. Differences between the results of methods 1 and 2 could occur if this assumption is incorrect. However, Figure 1 of Long et al. (2010) shows that most of the 137 known supernova remnants and SNR candidates in M33 are located on or close to $H\alpha$ emission. We used these data to construct the radial distribution of the number of SNRs/kpc² in M33 presented in Figure 2, which also shows the radial variation of the thermal emission. Out to $R = 5$ kpc, the radial distribution of the SNRs is very similar in shape to that of the thermal emission and has roughly the same scale length. As in the dense ISM near the centre not all SNRs may have been detected, the scale length of 2.9 ± 0.7 kpc may be an upper limit. Thus in M33 the distribution of the thermal emission may indeed be representative for the source distribution of CRE.

Recently, Tabatabaei et al. (2013a) estimated the diffusion length of CRE on small scales (< 1 kpc) in M31 and M33 from NTH–FIR correlations as a function of scale.⁴ They find $l_{\text{sky}} = 730 \pm 90$ pc for M31 and $l_{\text{sky}} < 400$ pc for M33. Their value for M31 is in excellent agreement with $l_{\text{sky}} = 715 \pm 20$ pc that we obtain from method 2, but their value for M33 is lower than our

⁴ Using a wavelet analysis, Tabatabaei et al. (2013a) decomposed each IR and radio map into a set of 6 (M31) or 7 (M33) maps each containing emission on a specific scale; the scales chosen are between 0.4 and 4 kpc. For each galaxy, maps on the same scale are then correlated and the derived correlation coefficients (r_w) are plotted as a function of scale. The smallest scale on which the synchrotron – 70 μm correlation has $r_w = 0.5$ is taken as the diffusion length of the CRE, because $r_w < 0.5$ implies that the correlation is lost, i.e. due to CRE diffusion and/or escape and turbulence in the ISM caused by SF regions and SNRs, synchrotron and 70 μm emission do not correlate on scales of $\lesssim 1$ kpc.

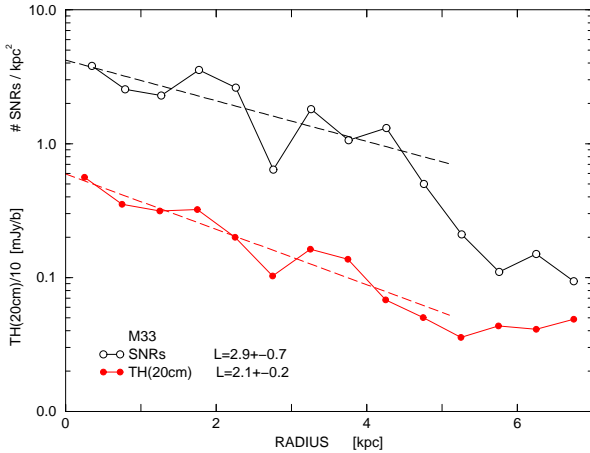


Figure 2. Radial distributions in M33: *black* – surface density of SNRs and SNR candidates of Long et al. (2010); *red* – surface brightness of thermal emission at 21 cm. Dashed lines are fits to the function $\exp(-R/L)$ with scale length L (in kpc) given in the figure. The similarity between the two distributions indicates that the the distribution of thermal emission is representative for that of the SNRs, the source distribution of the CRE.

upper limit of $l_{\text{sky}} = 900 \pm 110$ pc for the thin disk. As the authors explain, this low l_{sky} for M33 refers mostly to young CRE that are still close to their places of origin in the star forming regions. So their value may be considered a lower limit to l_{sky} of the bulk of CRE in M33. Since the emission from star forming regions occurs on small scales, their value is free from extended thick disk / halo emission.

5 DISTRIBUTION OF CRE IN M31 AND M33

Table 4 shows that at 1.4 GHz the diffusion length in the sky plane is about 1 kpc for M31 and about 1.5 kpc for M33. We have deprojected l_{sky} into the components $l_{x,y}$ in the plane of the galaxy and l_z perpendicular to the disk by assuming isotropy in the disk of the galaxy. Isotropy of CRE is consistent with the situation in the Milky Way where the diffusion of cosmic rays becomes isotropic on scales larger than 100–200 pc (Strong, Moskalenko & Ptuskin 2007; Dogiel & Breitschwerdt 2012), but below 1 kpc (Stepanov et al. 2012). Isotropy of CRE on large scales is also expected from simulations (Yan & Lazarian 2008).

We thus have $l_{\text{sky}} = l_x = l_y = l_z$, where l_x and l_y are measured along the major and minor axis in the plane of the galaxy, respectively, giving $l_{x,y} = l_x \sqrt{2}$ and $l_z = l_x$. This assumption leads to a circular extent of the propagation lengths on the sky plane, in agreement with the circular smoothing beams we derived. We present these values in Table 5.

In Table 5 we also give diffusion coefficients and confinement times of the CRE in the two galaxies. The diffusion coefficients in the x, y and z directions, $D_{\text{Ex,y}}$ and D_{Ez} , follow from Eq. 2 with the typical CRE ages $t_{\text{syn}}/2$ listed in Table 3. The confinement time is the time the CRE need to reach the scale height of the thin disk by diffusion, $t_{\text{conf}} = h_{\text{CRE}}^2/D_{\text{Ez}}$. We also list the mean velocities of the CRE when crossing the thin disk, $V_{\text{CRE}} = h_{\text{CRE}}/t_{\text{conf}}$. We discuss these results below. Note that since the diffusion lengths estimated by method 1 are upper limits, the values for the diffusion

coefficients also are upper limits,⁵ those for t_{conf} lower limits and those for V_{CRE} upper limits.

5.1 Confinement of CRE in M31

The diffusion length $l_{x,y}$ in the plane of M31 of about 1-2 kpc at 1.4 GHz is typical for galaxy disks (Murphy et al. 2006b). The corresponding diffusion coefficient of about $(1 - 3) 10^{28} \text{ cm}^2/\text{s}$ is in the range $10^{28} - 10^{29} \text{ cm}^2/\text{s}$ estimated for the Milky Way and other galaxies (e.g. Dahlem, Dettmar & Hummel (1994); Ptuskin & Soutoul (1998); Moskalenko et al. (2002); Murphy (2009); Heesen et al. (2009); Lacki & Thompson (2010), and references therein; Buffie, Heesen & Shalchi (2012); Tabatabaei et al. (2013b)).

Perpendicular to the disk the diffusion length at 1.4 GHz is only about 0.7 – 1.1 kpc. Since method 1 yields upper limits for the diffusion lengths, we use the smaller value of l_z of method 2 for comparison with the exponential scale height h_{CRE} given in Table 3. We convert the Gaussian-based value of l_z at 1.4 GHz to the exponential scale height⁶ $h_z = l_z/0.833 = 860 \pm 25$ pc, which is about 30 percent higher than the value of $h_{\text{CRE}} = 650 \pm 80$ pc given in Table 3. Both values refer to a mixture of CRE of all ages. Since h_{CRE} is derived from h_{syn} assuming energy equipartition between magnetic fields and CR particles, the fair agreement with h_z suggests that energy equipartition may indeed be valid for the radial range $R = 6.8 - 12.5$ kpc in M31.

The corresponding diffusion coefficient D_{Ez} of $0.45 10^{28} \text{ cm}^2/\text{s}$ is about half of $D_{\text{Ex,y}}$ and very low, indicating that CRE only slowly diffuse away from the midplane of the disk. The time the CRE need to move out of the thin disk, $t_{\text{conf}} = (2.8 \pm 0.7) 10^7$ yr, is close to the typical CRE age $t_{\text{syn}}/2 = (3.4 \pm 0.2) 10^7$ yr (see Table 3). Hence, the CRE have lost most of their energy before they can reach $z = h_{\text{CRE}}$ and only older CRE may move into a thick disk / halo, as the lower limit of t_{conf} of method 1 suggests. Thus, while the bulk of the CRE in M31 is confined to the thin disk (as shown by method 2), some of the older CRE may leave the thin disk at speeds of $V_{\text{CRE}} < 60 \pm 25 \text{ km s}^{-1}$. As this is about equal to the Alfvén speed⁷ of $V_A = 50 \pm 20 \text{ km s}^{-1}$, convective propagation of CRE by gas flows from SF regions does not play a role in M31.

Also Gräve, Emerson & Wielebinski (1981) and Berkhuijsen, Golla & Beck (1991) concluded that M31 does not have a thick disk / halo. The confinement of the CRE to the thin disk in M31 is consistent with the structure of the ordered magnetic field. Fletcher et al. (2004) found no significant vertical component of this field that is extraordinarily well aligned along the spiral arms in M31. The strong uniformity of the ordered field in the disk (Berkhuijsen, Beck & Hoernes 2003) probably leads to the small value of D_{Ez} and the confinement of the CRE to the thin disk.

⁵ Since method 1 refers to the older CRE, we should rather use $3t_{\text{syn}}/4$ than $t_{\text{syn}}/2$ to derive the diffusion coefficients, which would lower the upper limits by 30%. But in view of the large errors and for simplicity, we use $t_{\text{syn}}/2$.

⁶ As for a normalized Gaussian the halfwidth l occurs at $z=0.833$ and for a normalized exponential the scale height h is reached at $z = 1$, $h = l/0.833$.

⁷ We derived the Alfvén speed $V_A(\text{pc}/10^{-6} \text{ yr}) = B_{\text{perp,ord}}(\mu\text{G})/(4\pi < n_e > (\text{cm}^{-3})^{0.5})$, where $< n_e >$ is the density of free electrons in the ISM obtained from the mean rotation measure (Fletcher et al. 2004) and $B_{\text{perp,ord}}$ is the strength of the ordered magnetic field perpendicular to the LOS calculated from the polarized synchrotron emission.

Table 5. Diffusion lengths and confinement times of CRE in M31 and M33

GAL	M	FREQ [GHz]	$l_{x,y}^a$ [pc]	$D_{Ex,y}$ [10^{28} cm ² /s]	l_z^b [pc]	D_{Ez} [10^{28} cm ² /s]	t_{conf}^c [10^7 yr]	V_{CRE}^d [km s ⁻¹]
M31	1	1.465	1610 ± 280	2.3 ± 0.8	1140 ± 200	1.2 ± 0.4	1.1 ± 0.5	60 ± 25
		4.85	1390 ± 230	3.1 ± 1.1	980 ± 160	1.5 ± 0.5	0.6 ± 0.3	90 ± 40
	2	1.465	1010 ± 30	0.9 ± 0.1	715 ± 20	0.45 ± 0.03	2.8 ± 0.7	20 ± 6
		4.85	720 ± 90	0.8 ± 0.2	510 ± 60	0.41 ± 0.11	2.3 ± 0.9	25 ± 8
M33	1	1.425	1270 ± 160	1.9 ± 0.6	900 ± 110	1.0 ± 0.3	1.2 ± 0.6	50 ± 30
		8.35	1020 ± 130	2.9 ± 0.8	720 ± 90	1.4 ± 0.4	0.5 ± 0.3	100 ± 55
	2	1.425	2770 ± 240	9.3 ± 1.9	1960 ± 170	4.6 ± 0.9	0.3 ± 0.2	210 ± 120
		8.35	2050 ± 290	11.5 ± 3.5	1450 ± 200	5.8 ± 1.8	0.13 ± 0.08	380 ± 230

(a) $l_{x,y} = l_{\text{sky}} \sqrt{2}$

(b) $l_z = l_{\text{sky}}$

(c) $t_{\text{conf}} = h_{\text{CRE}}^2 / D_{Ez}$ (with h_{CRE} from Table 3)

(d) $V_{\text{CRE}} = h_{\text{CRE}} / t_{\text{conf}}$

5.2 Distribution of CRE in M33

An analysis of the polarized emission from M33 (Tabatabaei et al. 2008) revealed that the large-scale, ordered magnetic field in M33 has a vertical component of about $1 \mu\text{G}$, extending to at least $R = 5$ kpc. This implies that M33 has a nonthermal halo or thick disk containing CRE. In spite of this, the upper limits to the diffusion lengths obtained by method 1 (see Table 5) are smaller than the estimates of method 2, and even smaller than those of method 1 for M31. It seems that the halo contributions to the diffusion lengths at the two frequencies largely canceled in the difference Δl^2 (see Equation 5). We conclude that the results of method 1 apparently refer to the thin disk in M33. As the estimates of method 2 refer to thin+thick disk (Sect. 4), we discuss these cases separately.

THIN DISK. The upper limit to the diffusion length $l_{x,y}$ of 1.3 kpc at 1.4 GHz obtained from method 1 for the thin disk of M33 is about 30 percent smaller than that in M31 (see Table 5). As the stronger magnetic field B_{tot} (Table 3) yields smaller synchrotron loss times, the diffusion coefficient $D_{Ex,y}$ of $(1.9 \pm 0.6) 10^{28}$ cm²/s is similar to that in M31.

The upper limit to the diffusion length perpendicular to the disk of $l_z = 900 \pm 110$ pc and D_{Ez} are also similar within errors to those in M31 at 1.4 GHz. Here l_z corresponds to an exponential scale height $h_z = l_z / 0.833 = 1080 \pm 130$ pc, an upper limit consistent with the scale height $h_{\text{CRE}} = 620 \pm 150$ pc listed in Table 3. As the lower limit to the confinement time is about half of $t_{\text{syn}}/2$, some of the older CRE traced by method 1 may leave the thin disk at velocities of $V_{\text{CRE}} = 50 \pm 30$ km s⁻¹. Like in M31, this is equal to the Alfvén speed $V_A = 45 \pm 25$ km s⁻¹.

THIN+THICK DISK. At 1.4 GHz the diffusion length l_z of about 2 kpc, more than twice that of the thin disk, yields an exponential scale height of $h_z = 2350 \pm 280$ pc, corresponding to a synchrotron scale height of $h_{\text{syn}} = 2h_z / (3 + \alpha_n) = 1220 \pm 270$ pc. This value is consistent with the scale heights near 1 kpc in total emission observed in edge-on galaxies (Hummel, Beck & Dettmar 1991; Dumke et al. 1995), and confirms the existence of a thick synchrotron disk or halo in M33 (Tabatabaei et al. 2008). We may estimate the exponential scale height of the thick synchrotron disk by subtracting the contribution of the thin disk to h_{syn} , assuming that at $z=0$ kpc the intensities of thin and thick disk are equal. With $h_{\text{syn}} = 1.22 \pm 0.27$ kpc and $h_{\text{thin}} = 0.32 \pm 0.08$ kpc (Table 3), we find $h_{\text{thick}} = 2.1 \pm 0.5$ kpc at 1.4 GHz. This value of h_{thick} agrees with

the mean value of $h_{\text{thick}} = 1.8$ kpc in 5 galaxies (at 4.8 GHz) listed by Krause (2011). The agreement, however, may be fortuitous because (1) our estimate of h_{thick} in M33 is sensitive to the relative intensities of thin and thick disk at $z=0$ pc, and (2) the value of Krause (2011) refers to the sum of thermal and nonthermal emission instead of to nonthermal emission alone.

The value of D_{Ez} of $4.6 10^{28}$ cm²/s is nearly 5 times higher than in the thin disk. This leads to a confinement time of $t_{\text{conf}} = (0.3 \pm 0.2) 10^7$ yr that is significantly shorter than the typical CRE age $t_{\text{syn}}/2 = (2.5 \pm 0.2) 10^7$ yr. Hence, in M33 many CRE will move out of the thin disk into the thick disk / halo at a mean velocity of $V_{\text{CRE}} = 210 \pm 120$ km s⁻¹. This velocity is higher than the Alfvén velocity of about 50 km s⁻¹, suggesting that CRE are leaving the disk by a galactic wind.

As the older CRE traced by method 1 are largely confined to the thin disk, mainly young CRE are moving along the vertical magnetic field into the thick disk / halo. The multi-scale analysis of the NTH–FIR correlation in M33 of Tabatabaei et al. (2013a) indicates that CRE propagate from the star forming regions into the thick disk. Outflow of CRE and gas from bright SF regions is often observed in edge-on galaxies with a thick radio disk or halo (e.g. Dahlem, Lisenfeld & Golla (1995); Krause (2009); Heesen et al. (2009)). The outflow weakens the NTH emission from SF regions and decreases the dynamic range of the emission from the thin disk. CRE in the thick disk / halo also have velocity components parallel to the disk, leading to distribution of the CRE across the disk and further smoothing of the observed NTH emission (Breitschwerdt, Dogiel & Völk 2002; Dogiel & Breitschwerdt 2012). Hence, outflow of CRE from SF regions into the thick disk / halo mimics the effect of “horizontal” CRE diffusion in the thin disk.

The large value of $l_{x,y} \approx 2.8$ kpc obtained by method 2 at 1.4 GHz, more than twice as large as found for the thin disk, is consistent with the effects of CRE outflow described above. The smoothness of the observed NTH emission from the (thin + thick) disk of M33 is reflected in the large l_{sky} of about 2 kpc (Table 4) and in the low exponents b of the NTH–FIR correlations (Table 2).

6 DISCUSSION

In this section we discuss the effect of the superposition of the disk and halo emission in M 33 along the LOS as well as the influence of the magnetic field structure and of the star formation rate on the CRE distribution in M 31 and M 33.

6.1 Effect of the superposition on the sky of disk and halo emission

In Section 5.2 we have argued that M 33 has a nonthermal thick disk or halo. Since the inclination angle of M 33 is 56° , this means that on the sky plane we see the halo emission superimposed onto the more prominent disk emission. The addition of the distributions of two components generally leads to a smoother distribution than that of the individual ones. Therefore, the nonthermal emission observed on the sky will be smoother than that of the disk emission alone. This implies that the derived diffusion length will be larger than the actual diffusion length in the thin disk, because (using method 2) the TH emission needs to be more strongly smoothed to reach exponent $b=1$ in $NTH \propto TH^b$. This explains why in M 33 $l_{x,y}$ obtained by method 2 (Table 5) is larger than that of the thin disk found by method 1 although the CRE traced by method 2 are younger than those traced by method 1.

Possibly, not only $l_{x,y}$ but also l_z is larger than the actual propagation length perpendicular to the disk. In that case also the derived scale heights will be too high. Since we cannot separate the disk and halo emission from M 33, the values of method 2 given in Table 5 should be regarded as upper limits.

We conclude that for galaxies with a thick NTH disk or halo the apparent diffusion length estimated from a comparison with H α or FIR data may be considerably larger than the actual diffusion length of the CRE in the thin disk, and that also the extent of the thick disk / halo may be overestimated.

6.2 Importance of the magnetic field structure

The diffusion length $l_{x,y}$ in the thin disk of M 31 at 1.4 GHz is about 1.3 times that in M 33 (Table 5, method 1). This difference may be due to differences in the diffusion coefficient and synchrotron lifetime since $l = (D_E t_{\text{syn}}/2)^{0.5}$ (Eq. 2).

The propagation of CRE in the ISM is largely determined by their interaction with magnetic fields. The diffusion coefficient depends on both the turbulent and the ordered magnetic field strength. The ordered field, mainly running parallel to the disk, favours the propagation of CRE along the disk, while the turbulent field hinders the CRE in traveling long distances in one direction because they are scattered by the fluctuating magnetic field (MHD waves). Models of diffusive CR propagation indicate that $D_E \propto (B_{\text{tur}}/B_{\text{ord}})^{-2}$ (Chuvilgin & Ptuskin 1993; Breitschwerdt, Dogiel & Völk 2002; Yan & Lazarian 2004, 2008; Shalchi et al. 2010; Dogiel & Breitschwerdt 2012). Table 6 gives B_{tur} , B_{ord} and their ratio in the thin disks of M 31 and M 33. The higher B_{tur} and lower B_{ord} in M 33 yield a 2.3 ± 0.8 times higher value of $B_{\text{tur}}/B_{\text{ord}}$ and one would expect a 5.3 ± 2.6 times lower value of $D_{\text{Ex,y}}$ in M 33 than in M 31. However, the observed factor obtained from Table 5 is only 1.2 ± 0.6 , which suggests that other factors also play a role.

At a fixed frequency the synchrotron lifetime of the CRE scales with $B_{\text{tot}}^{-1.5}$ (Eq. 4), thus for the diffusion length we have $l \propto (B_{\text{tur}}/B_{\text{ord}})^{-1} B_{\text{tot}}^{-0.75}$. Therefore, we expect that in M 33 $l_{x,y}$ is 0.37 ± 0.13 times that in M 31, i.e. $l_{x,y} = 600 \pm 230$ pc, but this is

Table 6. Mean values of some relevant variables in M 31 and M 33

Variable	Unit	M 31	M 33
R	kpc	6.8 – 12.5	0 – 5
NTH(21 cm)	$\mu\text{Jy}/\text{kpc}^2$	7.3 ± 0.4	17.3 ± 0.8
α_n	–	0.92 ± 0.06	0.86 ± 0.08
B_{tot}	μG	6.6 ± 0.3	8.1 ± 0.5
B_{tur}	μG	5.0 ± 0.2	7.6 ± 0.5
B_{ord}	μG	4.3 ± 0.3	2.8 ± 0.3
$B_{\text{tur}}/B_{\text{ord}}$	–	1.2 ± 0.4	2.7 ± 0.3
TH(21 cm)	$\mu\text{Jy}/\text{kpc}^2$	1.1 ± 0.1	5.35 ± 0.95
$f_{\text{th}}(21 \text{ cm})$	%	13 ± 1	24 ± 4
SFR/ pc^2	$M_\odot \text{Gyr}^{-1} \text{pc}^{-2}$	0.6 ± 0.1	3.0 ± 0.6

about half the observed value of $l_{x,y} = 1270 \pm 160$ pc. Similarly, the observed value of l_z in the thin disk is about twice as large as expected from scaling with the value in M 31. As explained in Sect. 6.1, these larger values may result from the superposition of the disk and halo emission from M 33. Thus the superposition further increases (decreases) the upper limits (lower) limits obtained by method 1 (see Sect. 5).

We conclude that the differences in $D_{\text{Ex,y}}$, $l_{x,y}$ and l_z between the thin disks of M 31 and M 33 may be qualitatively understood as the combined effect of the different magnetic field structures in the two galaxies and the existence of a thick disk / halo in M 33.

We note that this is the first time that (a) diffusion lengths and diffusion coefficients of CRE in the thin disks of galaxies are derived based on the distributions of the NTH emission alone, and (b) it is shown that these quantities depend on the properties of the magnetic field as well as on the occurrence of convective transport of young CRE from bright SF regions into a thick disk / halo.

6.3 Influence of star formation

Above we have seen that M 31 has no significant vertical magnetic field and that most of the CRE are confined to the thin disk (Sect. 5.1). In M 33, however, CRE are leaving the bright SF regions along the vertical magnetic field into the thick disk / halo (Sect. 5.2).

Vertical magnetic fields are common in galaxies with thick radio disks (e.g. Krause (2009); Heesen et al. (2009)) and are often related with star forming regions. Dahlem, Lisenfeld & Golla (1995) first pointed out that thick radio disks occur in galaxies with a high star formation rate (SFR). Do M 31 and M 33 fit into this picture?

M 33 indeed has a higher SFR than M 31 (Verley et al. 2009; Tabatabaei & Berkhuijsen 2010). We have calculated the mean SFR/ pc^2 for the areas under consideration from the extinction-corrected H α maps, using the same procedure as Tabatabaei & Berkhuijsen (2010). The values given in Table 6 show that the SFR/ pc^2 in M 33 is 5 times higher than in the bright ring of M 31. Therefore, the mean TH and NTH surface brightnesses in M 33 are higher than in M 31 (see Table 6; Fig. 1) because it has more massive stars and SNRs per unit area, and a stronger total magnetic field.

Rossa & Dettmar (2003) analysed the occurrence of gaseous halos observed in H α using a sample of 74 normal spiral galaxies seen edge-on. They found that all galaxies with a SFR/ $\text{pc}^2 > (1.4 \pm 0.2) M_\odot \text{Gyr}^{-1} \text{pc}^{-2}$ show extra-planar diffuse emission from ionized gas at mean distances of 1 – 2 kpc from the galactic plane, whereas most galaxies with lower SFR/ pc^2 only have a

thin disk. According to this division, M31 has a thin disk in H α (SFR/pc² = (0.6 ± 0.1) M $_{\odot}$ Gyr⁻¹ pc⁻²) and M33 has a thick disk or halo (SFR/pc² = (3.0 ± 0.6) M $_{\odot}$ Gyr⁻¹ pc⁻²). Indeed, in M31 the $|z|$ -extent of the diffuse H α emission is less than 500 pc (Walterbos & Braun 1994) and, based on a power-spectrum analysis, Combes et al. (2012) suggested that M33 has a thick H α disk. Since galaxies with a thick disk in H α emission that have been observed in the radio regime also have a thick radio disk (Rossa & Dettmar 2003), we may expect that M33 has a thick radio disk or halo. Thus the expectations from H α observations are in full agreement with our results of a thin NTH disk in M31 and a thick NTH disk / halo in M33 (Table 5).

The SFR/area weakly influences the strength and structure of the magnetic field in a galaxy. A higher SFR/area generally increases the total and turbulent magnetic field with (SFR/area)^{0.2–0.4}, but hardly affects the ordered magnetic field (e.g. (Chyzy 2008; Krause 2009; Tabatabaei et al. 2013b)). This explains why M33 has a stronger B_{tur} than M31. The ordered magnetic field, however, is determined by various dynamical and environmental effects caused by e.g. galactic rotation, density waves, shear and anisotropic compressions in spiral arms (Fletcher et al. 2011). Although within a galaxy $B_{\text{tur}}/B_{\text{ord}}$ may increase with (SFR/area)^{0.3} (Chyzy 2008), the many factors influencing B_{ord} may be the reason that between galaxies the ratio $B_{\text{tur}}/B_{\text{ord}}$ seems independent of SFR (Krause 2009). For example, M51 has a 4 times higher SFR/pc² than M33 and strong magnetic fields, but the ratio $B_{\text{tur}}/B_{\text{ord}}$ is similar to that in M31 (1.4 compared to 1.2 ± 0.5, see Tabatabaei et al. (2013a)). The strong density waves in M51 may be responsible for this situation.

We have shown that the differences in diffusion length in the thin disks of M31 and M33 are the result of both the different properties of the magnetic field in the two galaxies and the existence of a thick disk / halo in M33, which is absent in M31. As the field properties not only depend on the SFR/area, a clear correlation between diffusion length in the thin disk and SFR/area is not expected. However, galaxies with SFR/area > 1.4 M $_{\odot}$ Gyr⁻¹ pc⁻² are likely to have a thick radio disk / halo. Then the estimated “diffusion” lengths will be larger than expected from random walk diffusion alone because they are the result of a combination of diffusion in the thin disk and propagation of CRE into and inside the halo (Sect. 5.2), and the superposition of disk and halo onto the sky plane (Sect. 6.1).

7 COMPARISON WITH EARLIER WORK

7.1 Smearing experiments

A number of authors estimated the diffusion length of CRE in nearby galaxies by smearing the distribution of the FIR emission until it looked similar to that of the emission at 1.4 GHz (e.g. Bica, Helou & Condon (1989); Marsh & Helou (1995, 1998); Murphy et al. (2006a,b)). However, these studies have several drawbacks: (1) IR images at 24 – 70 μm were used as the source distribution of the CRE. Although IR emission is usually well correlated with H α emission within galaxies (e.g. Leroy et al. (2009); Verley et al. (2009); Tabatabaei & Berkhuijsen (2010)), the influence of other dust heating sources than massive stars and of the dust distribution are not known. (2) Part of the total power emission observed at 1.4 GHz is thermal emission and its fraction varies across a galaxy. The inclusion of thermal emission leads to diffusion lengths that are too small by an amount depending on the thermal fraction and its distribution in the galaxy. Murphy et al. (2008)

did correct the total power emission for the thermal contribution, but they assumed 2 populations of CRE sources with different mean ages: one of young SNRs on scales \lesssim 1 kpc and a diffuse one on scales > 1 kpc where CRE are accelerated by interstellar shocks in the diffuse ISM. We think that there is insufficient evidence for diffuse CRE sources. (3) The role of magnetic fields was not taken into account. (4) The effect of a halo on the derived diffusion lengths was not considered.

Our study is free of these problems because it is based on properly separated thermal and nonthermal emission distributions across M31 and M33 (see Sect. 2). Moreover, the thermal distribution represents the source distribution of the CRE, and the magnetic field properties are known. Although the diffusion lengths on the sky of about 1 kpc in M31 and 1–2 kpc in M33 (Table 4) are in the range of 0.5 – 3 kpc derived from radio(1.4 GHz) – FIR studies (e.g. Murphy et al. (2006b)), our values are more reliable estimates of l_{sky} .

Murphy et al. (2006b, 2008, 2012) found a steep decrease of their “diffusion length” with increasing SFR/area. We note that all galaxies in their sample have a SFR/area > (1.4 ± 0.2) M $_{\odot}$ Gyr⁻¹ pc⁻², indicating that all these galaxies are expected to have a thick radio disk / halo (see Sect. 6.2). Therefore, their “diffusion length” l includes CRE propagation into the halo and inside the halo parallel to the disk, making their values larger than expected for diffusive propagation (Sect. 5.2 and Sect. 6.1). The authors could not find a mechanism that could explain the steep slope of their l – SFR/area relation, possibly because they neither included the important factor $B_{\text{tur}}/B_{\text{ord}}$ nor the effect of a thick disk / halo on the observed propagation lengths in their analysis. The strong dependence of their “diffusion length” on SFR/area may reflect the increasing importance of convection of CRE into a thick disk / halo by winds from the SF regions and increasing escape of CRE.

7.2 Implications for the radio – FIR correlation within galaxies

Our study of the radio – FIR correlations in M31 and M33 (Fig. 1, Tables 1, 2) confirms that TH emission is about linearly proportional to emission from warm dust (Xu et al. (1992); Hoernes, Berkhuijsen & Xu (1998); Hippelein et al. (2003)) and that the correlation between NTH emission at 1.4 GHz and dust emission follows a power law with exponent $b < 1$ (Hoernes, Berkhuijsen & Xu 1998). We have shown that the smaller value of b in M33 compared to that in M31 can be explained by the seemingly larger propagation length of the CRE in M33 than in M31. Galaxies with a thick radio disk / halo are expected to have smaller values of b because the combined effect of CRE diffusion in the thin disk and propagation of CRE into and inside the thick disk / halo leads to a smoother NTH distribution than diffusion in the thin disk alone. The superposition of disk and halo emission onto the sky further smooths the emission that is observed.

In this context, the work of Dumas et al. (2011) on the galaxy M51 is very interesting. They made pixel-to-pixel correlations between dust emission at 24 μm and 1.4 GHz radio continuum emission for different regions in M51: central disk, spiral arms, interarms and outer parts. Eye estimates of bisector slopes⁸ in their Fig. 11 yield for the exponent c in $I_{1.4\text{GHz}} \propto I_{24\mu\text{m}}^c$ the values $c = 0.4$ for the central region, $c = 0.7$ for the spiral arms and $c \approx 1$ for

⁸ Dumas et al. fitted $y(x)$ -regression lines instead of bisectors.

interarm and outer regions. Since the total 1.4 GHz emission contains thermal emission with $c = 1$, the values of $c < 1$ for the central region and the spiral arms imply that the exponent b in the power law between nonthermal emission and dust emission, $NTH_{1.4\text{GHz}} \propto I_{24\mu\text{m}}^b$, is even smaller than c , i.e. $b < 0.4$ for the central region and $b < 0.7$ for the arms. Berkhuijsen et al. (1997) and Fletcher et al. (2011) showed that M 51 has a thick NTH disk / halo extending to a radius of $> 3'$ from the centre. The high SFR of M 51 (Leroy et al. 2009) favours the propagation of CRE into and inside the thick disk / halo, which will influence the observed propagation length. The high magnetic field strengths of $15 - 30 \mu\text{G}$ (Fletcher et al. 2011) yield a mean free path of the CRE or diffusion length in the thin disk of a few hundred pc (Tabatabaei et al. 2013a), which means that few CRE will move into the interarm and outer regions. In these regions, where $c = 1$, also $b = 1$ suggesting that $I_{NTH,1.4\text{GHz}}$ and $I_{24\mu\text{m}}$ are directly proportional.

8 SUMMARY

We performed classical correlations between the thermal (TH) and nonthermal (NTH) components of the radio continuum emission at 21 cm (1.4 GHz) and one higher frequency and far infrared (FIR) dust emission from M 31 and M 33. In both galaxies, the TH emission is linearly correlated with the emission from warm dust ($24 \mu\text{m}$, $70 \mu\text{m}$), but the power laws of the NTH – FIR correlations have exponents $b < 1$ (Fig. 1; Tables 1, 2). The latter increase with increasing frequency; since the diffusion length of cosmic ray electrons (CRE) gets smaller towards higher frequencies, this is a direct indication that the propagation of CRE away from their places of origin causes $b < 1$. The power-law exponents of the $NTH_{1.4\text{GHz}} - \text{FIR}$ correlations for M 33 are significantly lower (≈ 0.4) than those for M 31 (≈ 0.6), suggesting that the propagation length of the CRE in M 33 is larger than in M 31.

We estimated the diffusion length of the CRE in two ways: (1) by smoothing the NTH emission at the higher frequency until the correlation with the NTH emission at 1.4 GHz had the power-law exponent $b = 1$, and (2) by smoothing the TH emission until the correlation with the NTH emission at the same frequency had $b = 1$, assuming that the TH emission represents the source distribution of the CRE, as is the case in M 33 (Fig. 2). Method 1 yields an estimate of the diffusion length of the older CRE within the thin disk of the galaxy and method 2 estimates the propagation length of the bulk of CRE (i.e. of all ages) resulting from the combination of diffusion in the thin disk and convective propagation (galactic wind) of CRE out of the thin disk into and within a thick disk / halo.

Our estimates for the propagation lengths of CRE are the first ones obtained from the distributions of the NTH components of the radio emission.

Our main results are summarized as follows:

1. In M 31 most of the CRE are confined to a thin NTH disk with an exponential scale height of $0.3 - 0.4 \text{ kpc}$ at 1.4 GHz, whereas in M 33 many CRE move out of the thin disk into a thick disk / halo with scale height $h_{\text{thick}} \approx 2 \text{ kpc}$ at 1.4 GHz. A thick NTH disk or halo in M 33 (but not in M 31) is consistent with the higher SFR in M 33 and the existence of a vertical magnetic field component.

2. The propagation of CRE from the SF regions into and inside the thick disk / halo, and the superposition of disk and halo emission on the sky lead to larger apparent propagation lengths in

M 33 than the diffusion lengths in M 31 along and perpendicular to the disk plane (method 2).

3. We showed that in case of random walk diffusion in the thin disk $l_{x,y} \propto (B_{\text{tur}}/B_{\text{ord}})^{-1} B_{\text{tot}}^{-0.75}$ is expected (Sect. 6.2), leading to a 3 times smaller value in M 33 than in M 31. However, the (deprojected) diffusion length in M 33 is only 30% smaller than that in M 31, i.e. $l_{x,y} = 1.3 \pm 0.2 \text{ kpc}$ and $l_{x,y} = 1.6 \pm 0.3 \text{ kpc}$ at 1.4 GHz, respectively (Table 5). The high value of $l_{x,y}$ in M 33 is due to the thick disk / halo emission seen superimposed onto the disk emission on the sky.

4. For galaxies with a thick disk / halo the apparent propagation length derived from smearing experiments may be considerably larger than the actual diffusion length in the thin disk.

We conclude that the spatial structure, strength and regularity of the magnetic field in a galaxy as well as the occurrence of a galactic wind causing a thick disk / halo determine the propagation of the CRE. Hence, the power-law exponent of the NTH – FIR correlation within a galaxy is the result of the properties of the magnetic field and the existence of a thick disk / halo.

ACKNOWLEDGMENTS

We thank Gabi Breuer⁹ for getting the tables in the correct format. We thank Marita Krause for useful comments on the manuscript. Critical comments of the referee, Andrew Strong, lead to a better description of the basic assumptions in the paper.

REFERENCES

- Basu A., Roy S., Mitra D., 2012, ApJ, 756, 141
 Beck R., Golla G., 1988, A&A, 191, L9
 Beck R., Krause M., 2005, Astronomische Nachrichten, 326, 414
 Bell E. F., 2003, ApJ, 586, 794
 Berezhko E. G., Völk H. J., 2004, A&A, 427, 525
 Berkhuijsen E. M., Bajaja E., Beck R., 1993, A&A, 279, 359
 Berkhuijsen E. M., Beck R., Hoernes P., 2003, A&A, 398, 937
 Berkhuijsen E. M., Golla G., Beck R., 1991, in IAU Symposium, Vol. 144, The Interstellar Disk-Halo Connection in Galaxies, Bloemen H., ed., pp. 233–236
 Berkhuijsen E. M., Horellou C., Krause M., Neiningen N., Poezd A. D., Shukurov A., Sokoloff D. D., 1997, A&A, 318, 700
 Beuermann K., Kanbach G., Berkhuijsen E. M., 1985, A&A, 153, 17
 Bica M. D., Helou G., 1990, ApJ, 362, 59
 Bica M. D., Helou G., Condon J. J., 1989, ApJ, 338, L53
 Breitschwerdt D., Dogiel V. A., Völk H. J., 2002, A&A, 385, 216
 Buffie K., Heesen V., Shalchi A., 2012, ArXiv e-prints
 Chuvilgin L. G., Ptuskin V. S., 1993, A&A, 279, 278
 Chyzy K. T., 2008, A&A, 482, 755
 Combes F., Boquien M., Kramer C., et al., 2012, A&A, 539, A67
 Condon J. J., 1992, ARA&A, 30, 575
 Dahlem M., Dettmar R.-J., Hummel E., 1994, A&A, 290, 384
 Dahlem M., Lisenfeld U., Golla G., 1995, ApJ, 444, 119
 de Jong T., Klein U., Wielebinski R., Wunderlich E., 1985, A&A, 147, L6
 Devereux N. A., Price R., Wells L. A., Duric N., 1994, AJ, 108, 1667

⁹ who sadly passed away on 2013 May 29th

- Dogiel V. A., Breitschwerdt D., 2012, in EAS Publications Series, Vol. 56, EAS Publications Series, de Avillez M. A., ed., pp. 61–71
- Dumas G., Schinnerer E., Tabatabaei F. S., Beck R., Velusamy T., Murphy E., 2011, *AJ*, 141, 41
- Dumke M., Krause M., 1998, in Lecture Notes in Physics, Berlin Springer Verlag, Vol. 506, IAU Colloq. 166: The Local Bubble and Beyond, D. Breitschwerdt, M. J. Freyberg, & J. Truemper, ed., pp. 555–558
- Dumke M., Krause M., Wielebinski R., Klein U., 1995, *A&A*, 302, 691
- Fitt A. J., Howarth N. A., Alexander P., Lasenby A. N., 1992, *MNRAS*, 255, 146
- Fletcher A., Beck R., Shukurov A., Berkhuijsen E. M., Horellou C., 2011, *MNRAS*, 412, 2396
- Fletcher A., Berkhuijsen E. M., Beck R., Shukurov A., 2004, *A&A*, 414, 53
- Freedman W. L., Wilson C. D., Madore B. F., 1991, *ApJ*, 372, 455
- Gordon K. D., Bailin J., Engelbracht C. W., et al., 2006, *ApJL*, 638, L87
- Gordon K. D., Engelbracht C. W., Fadda D., et al., 2007, *Publ. Astr. Soc. Pac.*, 119, 1019
- Gräve R., Emerson D. T., Wielebinski R., 1981, *A&A*, 98, 260
- Heesen V., Beck R., Krause M., Dettmar R.-J., 2009, *A&A*, 494, 563
- Helou G., Bica M. D., 1993, *ApJ*, 415, 93
- Helou G., Soifer B. T., Rowan-Robinson M., 1985, *ApJL*, 298, L7
- Heyer M. H., Corbelli E., Schneider S. E., Young J. S., 2004, *ApJ*, 602, 723
- Hippelein H., Haas M., Tuffs R. J., Lemke D., Stickel M., Klaas U., Völk H. J., 2003, *A&A*, 407, 137
- Hoernes P., Berkhuijsen E. M., Xu C., 1998, *A&A*, 334, 57
- Hoopes C. G., Walterbos R. A. M., 2000, *ApJ*, 541, 597
- Hughes A., Wong T., Ekers R., Staveley-Smith L., Filipovic M., Maddison S., Fukui Y., Mizuno N., 2006, *MNRAS*, 370, 363
- Hummel E., Beck R., Dettmar R.-J., 1991, *A&AS*, 87, 309
- Isobe T., Feigelson E. D., Akritas M. G., Babu G. J., 1990, *ApJ*, 364, 104
- Krause M., 2009, in *Revista Mexicana de Astronomia y Astrofisica Conference Series*, Vol. 36, *Revista Mexicana de Astronomia y Astrofisica Conference Series*, pp. 25–29
- Krause M., 2011, *ArXiv e-prints*
- Lacki B. C., Thompson T. A., 2010, *ApJ*, 717, 196
- Leroy A. K. et al., 2009, *AJ*, 137, 4670
- Leverenz H., Filipović M. D., 2012, *ApSS*, 338
- Long K. S., Blair W. P., Winkler P. F., et al., 2010, *ApJS*, 187, 495
- Lu N. Y., Helou G., Tuffs R., Xu C., Malhotra S., Werner M. W., Thronson H., 1996, *A&A*, 315, L153
- Marsh K. A., Helou G., 1995, *ApJ*, 445, 599
- Marsh K. A., Helou G., 1998, *ApJ*, 493, 121
- Moskalenko I. V., Strong A. W., Ormes J. F., Potgieter M. S., 2002, *ApJ*, 565, 280
- Murphy E. J., 2009, *ApJ*, 706, 482
- Murphy E. J., Braun R., Helou G., et al., 2006a, *ApJ*, 638, 157
- Murphy E. J., Helou G., Braun R., et al., 2006b, *ApJL*, 651, L111
- Murphy E. J., Helou G., Kenney J. D. P., Armus L., Braun R., 2008, *ApJ*, 678, 828
- Murphy E. J., Porter T. A., Moskalenko I. V., Helou G., Strong A. W., 2012, *ApJ*, 750, 126
- Nieten C., Neininger N., Guélin M., Ungerechts H., Lucas R., Berkhuijsen E. M., Beck R., Wielebinski R., 2006, *A&A*, 453, 459
- Niklas S., Beck R., 1997, *A&A*, 320, 54
- Paladino R., Murgia M., Helfer T. T., Wong T., Ekers R., Blitz L., Gregorini L., Moscadelli L., 2006, *A&A*, 456, 847
- Ptuskin V. S., Soutoul A., 1998, *A&A*, 337, 859
- Rossa J., Dettmar R.-J., 2003, *A&A*, 406, 493
- Shalchi A., Büsching I., Lazarian A., Schlickeiser R., 2010, *ApJ*, 725, 2117
- Stanek K. Z., Garnavich P. M., 1998, *ApJL*, 503, L131
- Stepanov R., Shukurov A., Fletcher A., Beck R., La Porta L., Tabatabaei F., 2012, *ArXiv e-prints*
- Strong A. W., Moskalenko I. V., Ptuskin V. S., 2007, *Annual Review of Nuclear and Particle Science*, 57, 285
- Tabatabaei F. S., Beck R., Krause M., et al., 2007a, *A&A*, 466, 509
- Tabatabaei F. S., Beck R., Krügel E., Krause M., Berkhuijsen E. M., Gordon K. D., Menten K. M., 2007b, *A&A*, 475, 133
- Tabatabaei F. S., Berkhuijsen E. M., 2010, *A&A*, 517, A77
- Tabatabaei F. S., Berkhuijsen E. M., Frick P., Beck R., Schinnerer E., 2013a, *ArXiv e-prints*
- Tabatabaei F. S., Krause M., Fletcher A., Beck R., 2008, *A&A*, 490, 1005
- Tabatabaei F. S., Schinnerer E., Murphy E. J., et al., 2013b, *A&A*, 552, A19
- Verley S., Corbelli E., Giovanardi C., Hunt L. K., 2009, *A&A*, 493, 453
- Völk H. J., 1989, *A&A*, 218, 67
- Wall J. V., 1979, *QJRAS*, 20, 138
- Walterbos R. A. M., Braun R., 1994, *ApJ*, 431, 156
- Warner P. J., Wright M. C. H., Baldwin J. E., 1973, *MNRAS*, 163, 163
- Xu C., Klein U., Meinert D., Wielebinski R., Haynes R. F., 1992, *A&A*, 257, 47
- Yan H., Lazarian A., 2004, *ApJ*, 614, 757
- Yan H., Lazarian A., 2008, *ApJ*, 673, 942
- Yun M. S., Reddy N. A., Condon J. J., 2001, *ApJ*, 554, 803